Journal of Materials Chemistry C

ROYAL SOCIETY OF CHEMISTRY

PAPER

View Article Online
View Journal | View Issue

Check for updates

Cite this: J. Mater. Chem. C, 2025, 13, 6257

Non-diffusive behavior of aluminum and yttrium dopants in ZrO_2/Al_2O_3 and ZrO_2/Y_2O_3 bilayer thin films†

Haengha Seo, Jonghoon Shin, Han Sol Park, Tae Kyun Kim, Heewon Paik, Haewon Song and Cheol Seong Hwang *

Received 20th November 2024,
Accepted 6th February 2025

DOI: 10.1039/d4tc04917a

rsc.li/materials-c

This study investigates the diffusive and non-diffusive behaviors of Al and Y dopants in ZrO_2/Al_2O_3 and ZrO_2/Y_2O_3 stacked thin films grown *via* atomic layer deposition (ALD), focusing on their interaction with the film's crystallization and grain growth. Contrary to the conventional diffusion theory, this work reveals that the diffusion in these nano-scale thin films is strongly influenced by the formation of through-grain structures rather than concentration gradients. Various thin film stacks analyzed by grazing incidence X-ray diffraction confirm this phenomenon. In the bilayer configurations, the Al and Y dopant layers do not diffuse into the adjacent ZrO_2 lattice since they do not necessarily interfere with the continuous grain growth of the ZrO_2 layer. However, when the dopant layers are embedded within the ZrO_2, which disrupt ZrO_2 grain growth at the insertion site, they must diffuse away to form the through-grains and thus lower the grain boundary energy. These findings indicate that the primary driving force for the Al and Y dopant diffusion in ZrO_2 thin films is lowering the grain boundary energy, not the concentration gradient. In contrast, thicker (>0.3 nm) Al–O layers maintain structural integrity and inhibit through-grain formation, resulting in no Al diffusion. These results offer insights for implementing dopant layers in various thin film applications.

Introduction

Solid-state diffusion, described by Fick's first and second laws, is a well-established material theory with far-reaching applications in diverse engineering fields, including semiconductor device fabrication.[1] The driving force for the diffusion is the spatial chemical potential gradient, which is the concentration gradient, in most cases, of the diffusing species. The diffusion coefficient represents the kinetic processes of the diffusing material and matrix. However, conventional diffusion theory for bulk materials is phenomenological, which may not precisely reflect the local atomic arrangements in nano-scale systems, such as thin films grown by atomic layer deposition (ALD).

ALD is the widely accepted thin film growth method in the semiconductor field, where atomically thin and conformal film deposition is necessary.[2–4] High dielectric constant (k) doped-ZrO_2 thin films as the capacitor dielectric films for dynamic random access memory (DRAM) are a typical example grown by ALD.[5] Although the stable phase of the bulk ZrO_2 at temperatures relevant to DRAM fabrication and operation is monoclinic with a k value < 20, the thin films ($<<$10 nm thickness) with tiny grain size have a tetragonal phase with a k value $\sim$40, suitable for DRAM capacitors.[6,7] However, the limited band gap ($\sim$5.5 eV) with unavoidable defect formation during the low-temperature processing ($<$600 °C) of the film inevitably has incurred the leakage current problem. Interposing a thin Al–O layer ($<$1 nm) or doping the ZrO_2 film with Al ions solved the leakage current problem, but it also invoked a lowered k value issue.[8–12] Therefore, adopting other stacked materials or seeking other dopants is actively being pursued.[12,13]

Nonetheless, all these nano-layer stacking or doping of aliovalent elements proceed in a layer-by-layer manner due to the layer-by-layer nature of ALD. In this case, the diffusion (or interdiffusion) of the doped species (*ca.* Al) into the neighboring matrix material (*ca.* ZrO_2) may deviate from the conventional diffusion behavior, depending on the local atomic structure of the matrix material. ALD oxide films with thickness $<<$10 nm generally have an amorphous structure, which is later crystallized by post-deposition annealing (PDA) or post-metallization annealing (PMA). The relatively open structure of an amorphous material may enhance the dopant diffusion compared with the crystalline matrix. However, numerous grain boundaries in the

Department of Materials Science and Engineering, and Inter-University Semiconductor Research Center, Seoul National University, Seoul 08826, Republic of Korea. E-mail: cheolsh@snu.ac.kr

† Electronic supplementary information (ESI) available. See DOI: https://doi.org/10.1039/d4tc04917a

nano-scale crystalline thin films may enhance the dopant diffusion. An even more complication of the diffusion of the dopant layers may arise from transforming the neighboring amorphous matrix into the crystalline material.

Recently, the authors reported counter-intuitive experimental results on the diffusion of the Al–O layer interposed at the middle position of the ZrO_2 film into the nearby ZrO_2 layers.[12] When the ALD cycle number of the Al–O layer was <3, resulting in an Al–O layer thickness of <0.3 nm, all the Al ions diffused into the ZrO_2 layers during PDA at 600 °C.[12] However, when the Al–O ALD cycle number was >3, the interposed Al–O (or Al_2O_3) layer remained intact with minimal diffusion.[12] This finding was counter-intuitive because the thicker Al–O layer corresponded to the higher Al-concentration gradient along the ZrO_2 film thickness direction, so it must have shown a higher diffusion. The density functional theory calculations evaluated the thermodynamic energy states of these diffused or undiffused Al–O layers, providing insights into this phenomenon.[12] However, the kinetic factors that may have an even higher importance in such nano-scale thin films under the dynamically varying environment, *e.g.*, *in situ* or *ex situ* crystallization of the ZrO_2 film, have not been appropriately addressed.

It was noted that the upper and lower ZrO_2 layers formed continuous grains across the total film thickness after PDA at 600 °C when the interposed Al–O layer diffused.[12] In contrast, they formed separate grains when the Al–O layer remained intact, which appeared reasonable considering the amorphous nature of the retained Al–O layer would prohibit the crystallographic continuity between the upper and lower ZrO_2 films. Nonetheless, it was unclear why the thinner Al–O layer could not similarly function because they might still form a continuous amorphous layer at the as-deposited state.

The authors' other recent study reported an *in situ* crystallization of the ZrO_2 film during the ALD at 250 °C, supposedly amorphous when deposited on the Si substrate directly, when it is grown on the crystalline ZrO_2 underlayer, formed by the first ALD and subsequent PDA at 600 °C.[14] It was wondered if one or two monolayers of the Al–O deposited on the crystalline ZrO_2 underlayer would impede the *in situ* crystallization of the overgrowing ZrO_2 layer. Examining the Al–O layer effects on the *in situ* crystallization may provide a clue to the above questions.

Depositing the Al–O layer outside the ZrO_2 film, *i.e.*, at the top or bottom position of the ZrO_2 film, and examining the diffusion behavior is another feasible method to examine the correlation between the Al-diffusion and ZrO_2 crystallization. Compared to the case with the Al–O layer being interposed between the two ZrO_2 films, the top or bottom deposited Al–O layer configuration must induce more active Al-diffusion into the nearby ZrO_2 films because all Al atoms must diffuse into one ZrO_2 film. However, as discussed later, no Al-diffusion occurred in this case. All these experimental results indicate that the governing factor that controls the Al-diffusion into the ZrO_2 layer is not the Al-concentration gradient or its diffusion coefficient in these nano-scale thin films. This work systematically examines the control factor.

The peak position shift in the grazing incidence X-ray diffraction (GIXRD) was adopted as the efficient method to identify the Al-diffusion because the substitution of Zr ions with Al ions in the ZrO_2 varies the lattice parameter due to their ionic radius difference (Al^{3+} 54 pm *vs.* Zr^{4+} 72 pm). This method was proven more accurate than the chemical composition depth profiles because of the generally very thin thickness of the films adopted in this study (<10 nm), severely limiting the chemical analysis's depth resolution. More detailed information about the GIXRD measurement process and calibration criteria used in this work is provided in ESI.†

For comparison, similar experiments were performed for the Y–O layer interposed into or deposited at the top or bottom of the ZrO_2 film, which was reported to diffuse into the ZrO_2 layers irrespective of its thickness.[12,14] Similar GIXRD experiments were also feasible to examine the Y diffusion due to the substantial ionic radii difference (Y^{3+} 90 pm *vs.* Zr^{4+} 72 pm).

Results and discussion

Ionic radii of Al^{3+} (54 pm) and Y^{3+} (90 pm) ions are smaller and larger, respectively, than that of the Zr^{4+} ion (72 pm). When these dopant ions replace Zr ions in the crystal lattice of ZrO_2, the lattice constant varies.[12,14] GIXRD provides direct information about the lattice constant variation, which can infer the degree of Al and Y diffusion into the ZrO_2 film. Due to its high intensity, the tetragonal (111) diffraction peak is useful for analyzing ZrO_2 thin films in GIXRD. However, it is necessary to confirm that the doping changes the other interplanar spacings. Therefore, the same analysis was conducted on the (200) and (220) peaks alongside the (111) peak to address. The (111), (200) and (220) peak positions (2θ) of bulk tetragonal ZrO_2 are reported to be $\sim30.3^\circ$, $\sim35.3^\circ$ and $\sim50.6^\circ$, respectively (JCPDS 14-0534) for the Kα Cu X-ray radiation (1.5406 Å). Besides, the 2θ values of the ZrO_2 film (and other thin films) are also influenced by the intrinsic growth strain and extrinsic thermal strain, depending on the fabrication process.[14–17] Therefore, inferring the doping effect from the 2θ value variation must consider these factors carefully. These factors are considered in the following discussions.

In GIXRD, the diffracting planes are inclined from the surface-normal direction by (θ – incident angle). Consequently, the three peaks mentioned earlier must be oriented in different directions at any given incident angle. Measurements were taken at specific incident angles for each peak to eliminate this geometrical effect: the (111) peak at 0.5°, the (200) peak at 2.5° and the (220) peak at 10.0°. As illustrated in Fig. 1(a), this adjustment ensures that the diffracting planes in each analysis are equally inclined by $\sim15^\circ$ (θ – incident angle) from the film surface-normal direction.

Fig. 1(b) illustrates the change in the tetragonal ZrO_2(111), (200) and (220) diffraction peak positions of the 9–10 nm-thick ZrO_2 films deposited on Si substrates as a function of the number of ALD cycles of the Al–O and Y–O interlayers inserted in the middle region of the ZrO_2 film. The thicknesses of Al–O and Y–O interlayers correspond to ~0.10 nm and ~0.15 nm per ALD cycle, respectively. Since the as-deposited ZrO_2 films

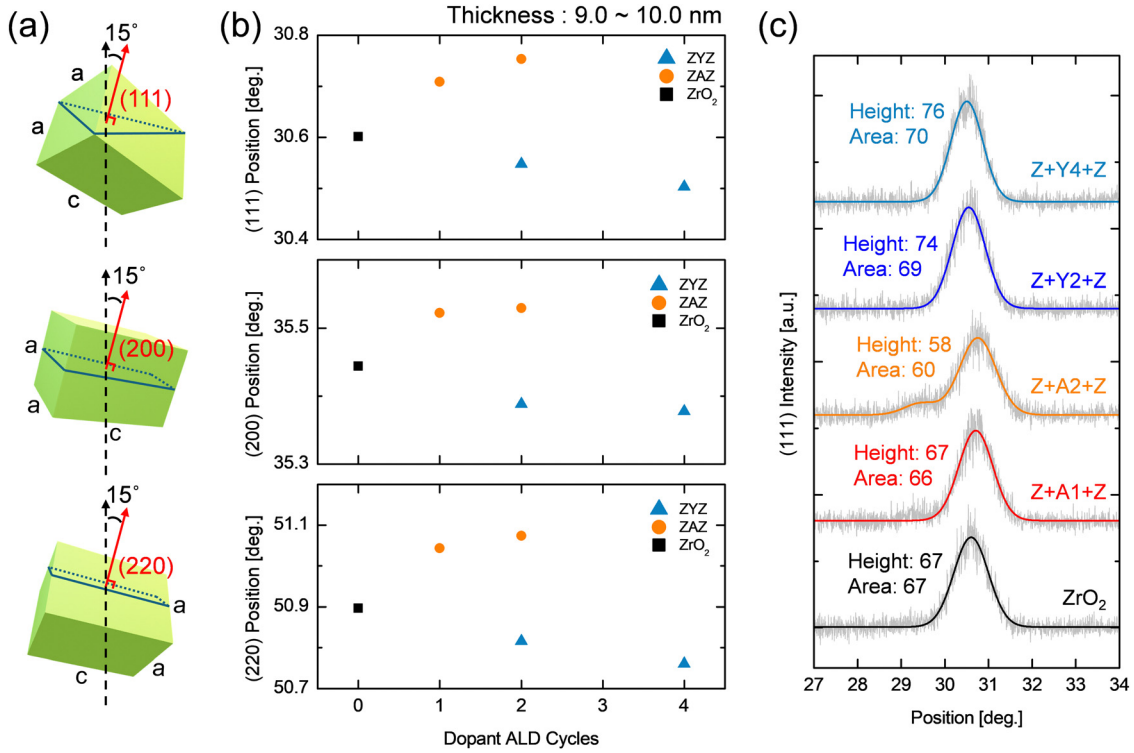

Fig. 1 (a) Schematic illustrations of the tetragonal ZrO_2(111), (200) and (220) diffracting planes within the unit cell, which are equally inclined by ~15° from the film surface-normal direction. (b) Changes in the diffraction peak positions (2θ) of the 9~10 nm-thick ZrO_2 films as functions of the number of Al or Y dopant ALD cycles inserted in the middle region. All diffraction peaks were measured *via* GIXRD and Gaussian fitted. (c) Raw data for the (111) diffraction peaks and the corresponding Gaussian-fitted lines.

were amorphous, all samples underwent PDA at 600 °C for crystallization. The total thickness and the deposition process for each sample were kept identical to avoid the involvement of growth or thermal strains.

Similar results are observed across all three peak position measurements. The ZrO_2/Al–O/ZrO_2 (ZAZ) film shows an increasing trend in 2θ with the number of interlayer ALD cycles compared to the 2θ of the undoped ZrO_2 film. According to Bragg's law, an increasing 2θ implies a decrease in the interplanar spacing of the diffracting planes, which stems from the substitutional diffusion of Al (with smaller ionic radius) ions into the ZrO_2 film. Conversely, the ZrO_2/Y–O/ZrO_2 (ZYZ) film shows a decreasing trend in 2θ with the increasing Y–O ALD cycles, indicating the increase in the (111) lattice spacing. This increase must be ascribed to the substitutional diffusion of Y (with larger ionic radius) ions into the ZrO_2 film.

The calculated interplanar spacings (d) and strain values for the three diffracting planes are listed in Table 1. The lattice constant changes for these three planes are consistent for each sample. This result suggests that diffused Al contracts the ZrO_2 unit cell in all three directions while diffused Y expands it.[12,14] Therefore, the strain caused by doping must be an isotropic change, different from growth and thermal strains, which typically evolve according to the Poisson effect.

Fig. 1(c) shows the raw data for the (111) diffraction peaks and the corresponding Gaussian-fitted lines. It can be seen that the peak intensity and area (values in arbitrary units) of ZAZ slightly decrease with the increasing number of Al–O cycles, indicating that the Al–O interlayer adversely affects the overall crystallinity. In contrast, ZYZ's peak intensity and area slightly increase with the increasing Y–O layer cycles. This finding, also reported by Seo *et al.*[12] indicates that an additional lattice of $Zr_{1-x}Y_xO_2$ was formed near the Y–O interlayer site during crystallization.

Table 1 Interplanar spacings (d) and strain values, extracted from the tetragonal ZrO_2(111), (200) and (220) diffraction peaks

	(111)		(200)		(220)	
	d (Å)	Strain (%)	d (Å)	Strain (%)	d (Å)	Strain (%)
ZrO_2 (9.5 nm)	2.921	—	2.533	—	1.794	—
Z+A1+Z	2.911	−0.340	2.527	−0.213	1.789	−0.268
Z+A2+Z	2.907	−0.482	2.527	−0.233	1.788	−0.323
Z+Y2+Z	2.926	0.171	2.536	0.152	1.797	0.148
Z+Y4+Z	2.931	0.314	2.537	0.181	1.799	0.250

A similar analysis was performed for the ZrO_2 films with the Al–O or Y–O layers deposited either on top (ZA and ZY) or at the bottom (AZ and YZ) of the ZrO_2. Fig. 2(a) shows the changes in the tetragonal ZrO_2(111) diffraction peak positions (2θ) as functions of the number of Al or Y dopant ALD cycles deposited on top of the ~7 nm-thick ZrO_2 (upper panel) or at the bottom of the ~6 nm-thick ZrO_2 films (lower panel). Interestingly, no 2θ shift was observed with the increasing dopant ALD cycles for these bilayer stacks, regardless of the dopant element, even

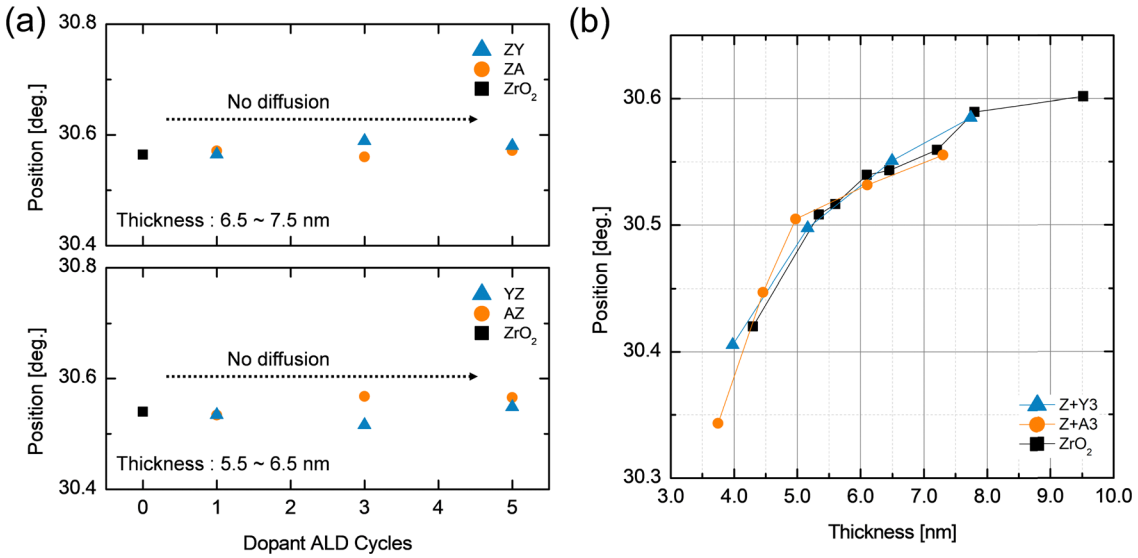

Fig. 2 (a) Changes in the tetragonal ZrO_2(111) diffraction peak positions (2θ) as functions of the number of Al or Y dopant ALD cycles inserted on top of the ~7 nm-thick ZrO_2 (upper panel) and at the bottom of the ~6 nm-thick ZrO_2 films (lower panel). All diffraction peaks were measured *via* GIXRD at an incident angle of 0.5° and Gaussian fitted. No position changes in both bilayer stacks indicate no dopant diffusion into the ZrO_2. (b) Changes in the (111) diffraction peak positions (2θ) of the ZrO_2, Z+A3 (3 Al–O on top) and Z+Y3 (3 Y–O on top) films as functions of the film thickness.

after the same PDA. This finding indicates an absence of the diffusion-induced lattice parameter change in both cases. Therefore, it can be concluded that Al or Y diffusion (*i.e.*, ion substitution) into the nearby ZrO_2 lattice does not occur when the dopant layer is located outside the ZrO_2 layer. Such non-diffusive behaviors were also observed when the same experiment was conducted by depositing the dielectric film on a sputtered 50 nm-thick TiN layer (ESI†).

Fig. 2(b) shows the variations in the (111) diffraction peak positions (2θ) of the pure ZrO_2, Z+A3 (3 Al–O on top of ZrO_2) and Z+Y3 (3 Y–O on top of ZrO_2) films as functions of the film thickness. It should be noted that the peak position is significantly dependent on the film thickness when the film is only a few nanometers. In this thickness range, the growth stress evolves as a function of thickness and ultimately affects the net internal strain state.[14–17] The peak position of the pure ZrO_2 films (black square) increases with the increasing film thickness due to the evolution of the growth strain.[12,14] Thus, when comparing peak positions due to dopant diffusion, it is essential to compare only films of similar thicknesses to exclude the growth strain effect. The Z+A3 and Z+Y3 films exhibit trends similar to the pure ZrO_2 case with only marginal deviations, again confirming that the outer dopant interlayers did not diffuse, regardless of the film thickness.

The following experiment investigated these contrasting diffusion characteristics occurring when the interlayer is positioned inside or outside the ZrO_2 film. Initially, while maintaining the overall thickness of the film constant, the diffusion behavior according to the positional variation of a 2-cycle Al–O interlayer from the top surface or bottom interface towards the bulk ZrO_2 interior was examined by tracing the changes in (111) diffraction peak position. Fig. 3(a) illustrates the variation in 2θ

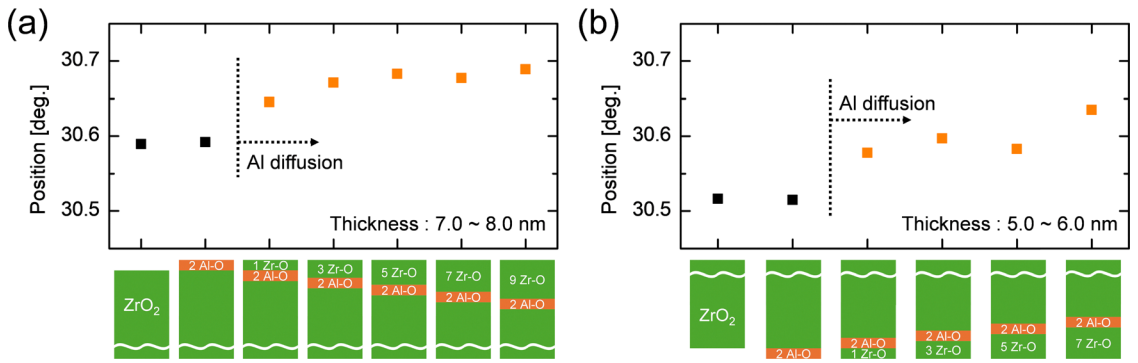

Fig. 3 Changes in the tetragonal ZrO_2(111) diffraction peak positions (2θ) in response to the positional variation of a 2-cycle Al–O interlayer in the ZrO_2 thin films; (a) from the top surface for a fixed total thickness of 7~8 nm and (b) from the bottom interface for a fixed thickness of 5–6 nm, while maintaining the overall thickness of each ZrO_2 film constant. All film stacks were PDA treated, and the diffraction peaks were measured *via* GIXRD at an incident angle of 0.5° and Gaussian fitted.

when the Al–O interlayer position varies from the top surface (total thickness of 7–8 nm). In contrast, Fig. 3(b) shows similar results when the Al–O interlayer position varies from the bottom interface (total thickness of 5–6 nm). Each film configuration is schematically depicted in the lower portion of the figures. The adopted ZrO_2 film thickness in Fig. 3(b) is slightly thinner than in Fig. 3(a), considering the relatively lower contribution of the doping-induced strain effect present in the lower region due to the surface-sensitive nature of GIXRD. In Fig. 3(a), when the 2-cycle Al–O was positioned outermost (on the ZrO_2 surface), no change in 2θ was observed, similar to the results in Fig. 2(a). However, upon depositing only one cycle of Zr–O covering the Al–O interlayer, a measurable increase in 2θ was noted, indicating substantial Al diffusion. As the Al–O layer was placed further into the ZrO_2 interior, a progressive increase in 2θ was observed. This finding signifies that diffusion became more pronounced with deeper placement of the Al–O layer into the ZrO_2. When assuming the equivalent diffusion of Al atoms into the upper and lower portions of the ZrO_2 film, the lack of sufficient ZrO_2 material in the upper portion for the 1 or 3 Zr–O cycle on the Al–O cycle sample may induce lower overall Al diffusion.

The same results were observed when the 2-cycle Al–O layer was located under the ZrO_2 layer (Fig. 3(b)). As shown in Fig. 2(a), when the interlayer was entirely outside the ZrO_2, there was no change in 2θ. However, an apparent increase in 2θ due to Zr–Al interdiffusion was observed once a single Zr–O cycle was deposited below the Al–O interlayer. 2θ value further increased as the Al–O layer was positioned deeper into the ZrO_2 interior. This increase can also be understood as the Zr–O layer deposited below the Al–O layer was too thin for Al ions to diffuse downward. Therefore, Fig. 3(a) and (b) conclude that Al diffusion into the nearby ZrO_2 lattice occurs in both upward and downward directions as long as the Al–O layer is inside the ZrO_2 film. Notably, only a single Zr–O ALD cycle ($\sim$0.1 nm-thick ZrO_2) outside the Al–O layer also induces substantial Al diffusion.

The following experiments were performed to clarify why the bidirectional Al diffusion occurs only when the dopant layer is embedded inside the bulk ZrO_2 but not when it is outside. The experimental design was based on the idea that two separated ZrO_2 layers, no matter how thin, tend to form continuously crystallized grains (*i.e.*, "through-grains") during PDA to minimize the interface energy. When the interposed Al–O layer interferes adversely with the through-grain formation, the driving force for the through-grain formation induces the Al diffusion. When the Al–O layer resides outside the ZrO_2 film, it has no crystallization interference effect, so there is no Al diffusion.

As-deposited ZrO_2 thin (<10 nm) films on Si substrates are initially in an amorphous state and require PDA (600 °C) for crystallization. However, it was reported that ZrO_2 thin films could undergo *in situ* crystallization *via* local epitaxy on an already crystallized seed ZrO_2 layer.[14] For such an *in situ* crystallization, a 5 nm-thick ZrO_2 film was deposited and underwent PDA to form the crystallized seed layer, which served as a template for local epitaxial growth. Then, the upper

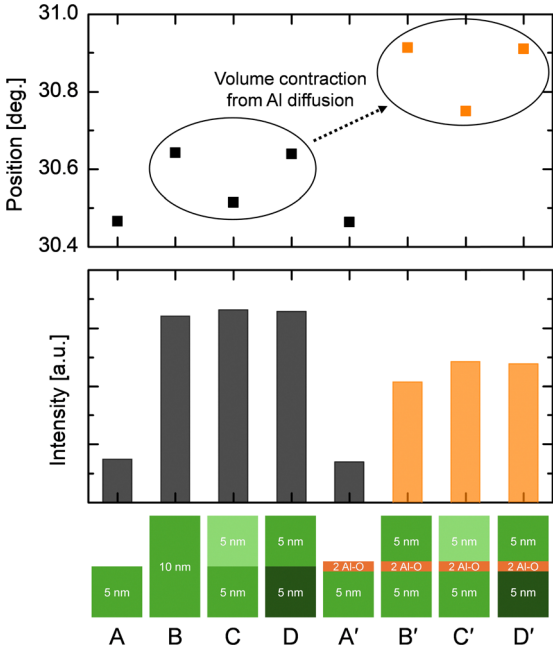

Fig. 4 Tetragonal ZrO_2 (111) diffraction peak positions (2θ) and intensities of the various ZrO_2 film stacks with or without the 2-cycle Al–O layer. All diffraction peaks were measured *via* GIXRD at an incident angle of 0.5° and Gaussian fitted. The brightest ZrO_2 blocks in the illustrations represent *in situ* grown layers without PDA treatment deposited on the already crystallized seed layer. The medium-colored blocks represent the layers crystallized *via* PDA, and the darkest blocks represent the layers subjected to PDA twice. The orange-colored points and bars indicate that the Al–O layer in the film stack was diffused.

layer was deposited using the identical ALD process at 250 °C, which was crystallized without further PDA. This method resulted in the upper ZrO_2 layer exhibiting equivalent crystallinity to the PDA-treated ZrO_2.[14] Based on this report, the effect of the interposed 2-cycle Al–O layer between the seed and upper layer on the crystallization of the double-layer ZrO_2 film was examined.

Fig. 4 shows the (111) diffraction peak positions and intensities of eight types of film stacks. The seed (lower) layers were fixed at $\sim$5 nm and crystallized *via* PDA. Samples A and B are single-step PDA-treated ZrO_2 films with 5 nm and 10 nm thicknesses, respectively. Sample C is a 10 nm-thick ZrO_2 film, with a 5 nm-thick upper layer deposited on a PDA-treated seed layer. Subsequently, sample C underwent PDA treatment again, resulting in sample D. In the figure, the brightest ZrO_2 blocks represent *in situ* grown layers without PDA treatment. The medium-colored blocks represent layers crystallized *via* PDA, and the darkest blocks represent layers subjected to PDA twice. It can be observed that samples B, C and D exhibit the same peak intensities (and also the peak shapes, data not shown), again confirming the equivalent crystalline structure of the *in situ* crystallized upper layer compared to the conventional PDA-treated ZrO_2 layer. However, according to the previous report,[14] the thermal expansion coefficient mismatch between the ZrO_2 layer and the Si substrate resulted in additional lateral tensile strain (and vertical compressive) in the PDA-treated

ZrO_2 layers. Naturally, this extrinsic tensile strain was absent in the *in situ* crystallized upper layer.[14] The lower 2θ value of sample C compared to samples B and D further corroborates this finding. Considering that the diffracting planes are inclined by 15° from the surface-normal direction, it can be inferred that lower 2θ values reflect less tensile (or more compressive) strain imparted laterally in the film. It should also be noted that sample B exhibits a higher 2θ value than sample A, signifying more (lateral) tensile strain attributed to the intrinsic growth tensile strain resulting from Volmer–Weber type film growth.[14–17]

For comparison, a 2-cycle Al–O layer was introduced on top of the seed layer in each sample before undergoing the seed-layer PDA treatment (samples A′–D′). Comparing samples A and A′, as expected, the Al–O layer outside the ZrO_2 was not diffused, resulting in identical 2θ and intensity values. The peak intensity increased when the upper layer was subsequently grown on top of sample A′, corresponding to sample C′. This finding indicates that the upper layer was crystallized following local epitaxy despite the presence of the Al–O layer. In other words, the 2-cycle Al–O layer could not obstruct the local epitaxy from the ZrO_2 seed layer, allowing the upper layer to crystallize. Furthermore, the intensity level is comparable to sample B′, a 10 nm-thick single-step PDA-treated ZAZ film with the Al–O layer incorporated within the bulk ZrO_2. As shown by samples B and C, even when crystallization occurred *via* local epitaxy, the degree of crystallization remained consistent.

Comparing the peak position of sample C′ to sample C reveals a significant increase in 2θ. This finding suggests that the Al–O layer, which had not diffused in sample A′, did diffuse

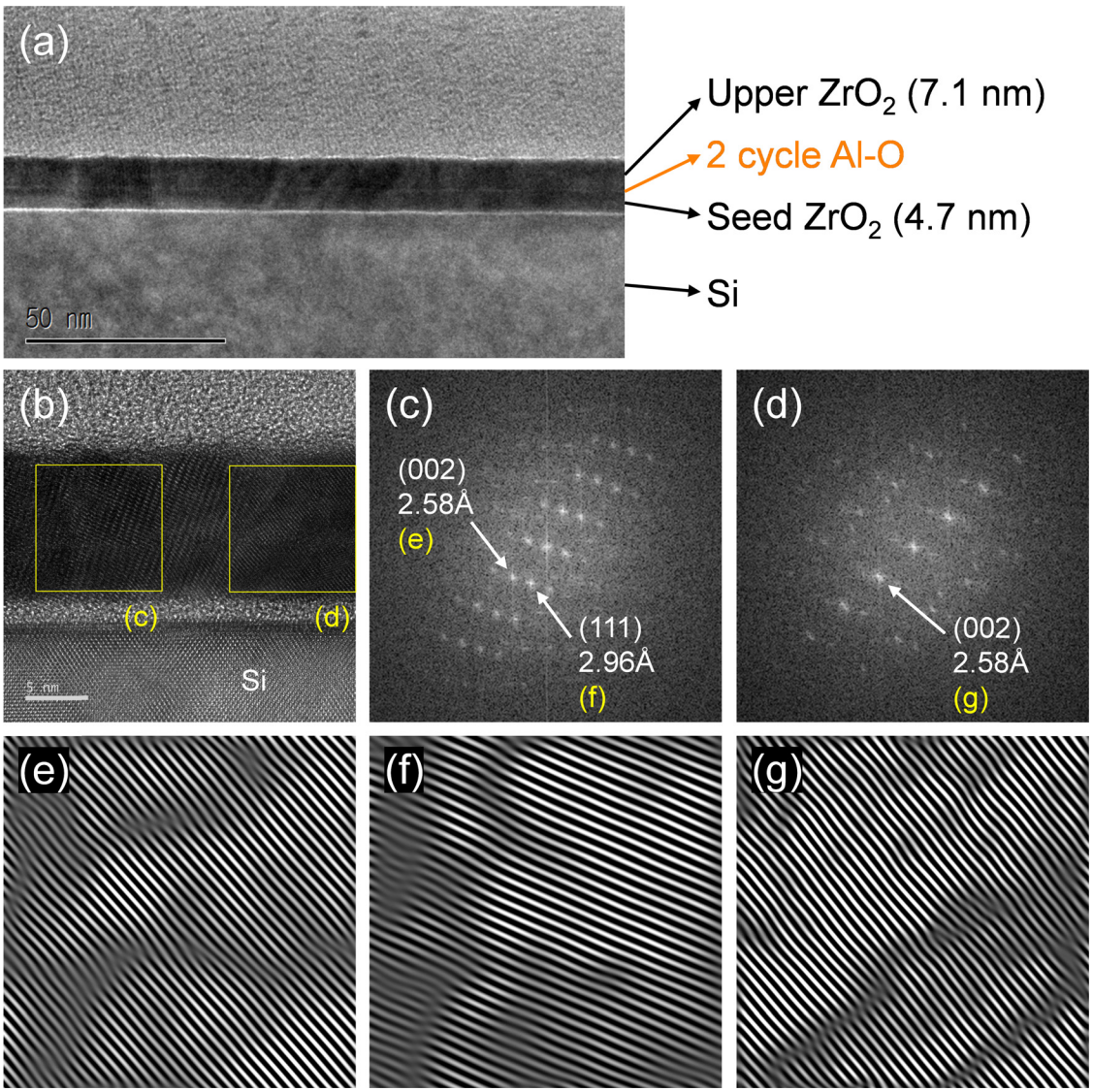

Fig. 5 TEM images of the seed-layered 11.8 nm-thick ZrO_2 film. A 2-cycle Al–O layer was inserted between the 4.7 nm-thick seed ZrO_2 and the 7.1 nm-thick upper ZrO_2 layers. (a) Bright field image showing the brighter contrast line near the Al–O layer site. (b) High-resolution image showing the through-grain lattice fringes. The regions marked with yellow boxes were selected for FFT image processing in (c) and (d). (e)–(g) Inverse-FFT images of the selected (111) and (002) diffraction spots from (c) and (d).

once the upper layer was epitaxially grown on top. It can be understood that regardless of the grain growth method, the advancing grains should break down the thin dopant layer through Zr–Al interdiffusion, forming the through-grains when a dopant layer presents inside the ZrO_2 films.

Additionally, the 2θ difference due to the absence of thermal tensile strain in the upper layer, as discussed for sample C, was similarly observed in sample C′. Samples B′, C′ and D′ exhibited the same internal strain evolution as their counterparts, samples B, C and D, with the added effect of lattice parameter contraction induced by Al diffusion. Furthermore, the Al–O layer hindered overall crystallinity, reducing peak intensity compared to the undoped sample group, irrespective of the crystallization method employed.

Fig. 5 shows the transmission electron microscopy (TEM) images of the 11.8 nm-thick ZrO_2 film deposited through the following process: A 2-cycle Al–O layer was deposited on a 4.7 nm-thick seed ZrO_2 layer, followed by PDA for crystallization. Subsequently, a 7.1 nm-thick upper ZrO_2 layer was deposited to induce *in situ* crystallization. As the upper ZrO_2 forms the through-grains with the seed ZrO_2 layer, the Al–O layer is expected to diffuse into the adjacent ZrO_2 lattice. In the low magnification image of Fig. 5(a), a brighter contrast line is visible near the position of the 2-cycle Al–O layer. However, this contrast does not represent a distinct Al_2O_3 layer but indicates a higher Al-concentration near the deposition site, similar to observations in Y-doped ZrO_2 films elsewhere.[12] Fig. 5(b) shows an enlarged high-resolution TEM image displaying the lattice fringes, where it can be observed that the upper ZrO_2 has formed the through-grains with the seed ZrO_2 layer. The regions marked with yellow boxes were selected for fast Fourier transform (FFT) image processing, as shown in Fig. 5(c) and (d). Fig. 5(e)–(g) present the inverse-FFT images of the selected (111) and (002) diffraction spots from Fig. 5(c) and (d). These images commonly demonstrate the presence of continuous grains throughout the entire film thickness.

Seo *et al.* reported that an Al–O layer thicker than 0.3 nm inserted in the middle region of the ZrO_2 film formed a continuous Al–O (or Al_2O_3) layer, effectively separating the upper and lower portions of the ZrO_2 film.[12] As a result, the upper and lower ZrO_2 layers crystallized distinctly. It was also found that the Al ions did not diffuse into either of them once they were separated, even when the Al–O layer was sufficiently thick. This phenomenon can also be interpreted using the assumptions made earlier. When the Al–O interlayer is thick enough to interfere with the continuous crystallization of the upper and lower portions (so that the upper and lower portions crystalize separately), the Al–O layer remains intact without interdiffusion. In this case, the system energy must be higher than the through-grain film due to the presence of the two ZrO_2/Al–O interfaces. Therefore, a higher PDA temperature may induce interdiffusion.

In contrast, thicker Y–O interlayers (even as thick as 1.5 nm) facilitated continuous ZrO_2 grain formation despite the locally higher Y-concentration at its inserted location.[12] The Y–O layer did not form an independent Y_2O_3 layer, even though its thickness of ~1.5 nm was well above the typically expected monolayer thickness, which would be sufficient to fully cover the bonding environment of the underlying ZrO_2. The Y_2O_3–ZrO_2 phase diagram shows extensive solid solubility of Y ions in ZrO_2, facilitating the interdiffusion between them.[18] In contrast, the Al_2O_3–ZrO_2 phase diagram reveals almost no solid solubility between them.[19] Therefore, even the thicker Y–O interlayer does not interfere with the continuous crystallization of the ZrO_2 film (forming the through-grains), as the interposed Y–O layer readily diffuses away from its location. Interestingly, such a facile Y–Zr interdiffusion does not occur when the Y–O layer presents outside the ZrO_2 film, as shown next.

The undoped ZrO_2 film crystallizes under the given PDA condition when thicker than ~3.5 nm (critical thickness).[12] Fig. 6(a) shows the GIXRD pattern of the 3.0 nm-thick ZrO_2 single layer (25 Zr–O cycles, named "Z25") after PDA, indicating that it is almost amorphous due to its thinness. Fig. 6(b) shows the data for a 4.3 nm-thick ZrO_2 single layer (35 Zr–O cycles, named "Z35"), indicating that it is crystalline as it exceeds the critical thickness. Fig. 6(c) shows the data for a 10-cycle Y–O layer (1.4 nm) deposited on the Z25 film (named "Z25Y10") after PDA, indicating the stacked layer remained almost amorphous. As the total film thickness is 4.4 nm, over the critical thickness, it must have been crystallized if the two layers intermixed and formed a solid solution. This finding indicates that the upper Y–O layer remained unmixed with the underlying ZrO_2 layer in this sample configuration despite its high diffusivity and solid solubility. In contrast, the similar 10-cycle Y–O layer (1.4 nm) intervened between the bottom 13-cycle ZrO_2 (1.6 nm) and top 12-cycle ZrO_2 (1.5 nm) layers (named

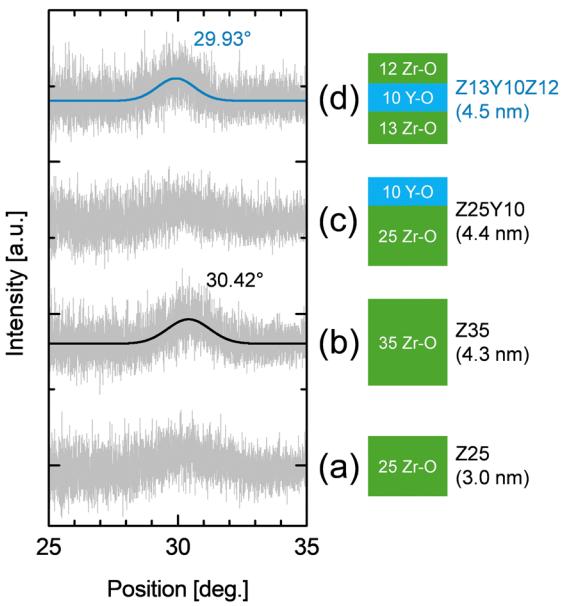

Fig. 6 (a)–(d) GIXRD spectra showing the tetragonal ZrO_2(111) diffraction peaks of the various ZrO_2 film stacks with or without the 10-cycle Y–O layer (1.4 nm). All film stacks were PDA treated, and the diffraction peaks were measured at an incident angle of 0.5° and Gaussian fitted. The Y–O layer was diffused only in the Z13Y10Z12 film, followed by the ZrO_2 grain growth.

"Z13Y10Z12") appears to be mixed with the nearby ZrO_2 layers forming a 4.5 nm-thick crystalline solid solution film, as shown in Fig. 6(d). Therefore, Y–O has a similar property to Al–O regarding diffusion depending on the through-grain formation. The larger Y ionic size increases the unit cell parameter, and the (111) peak position shifts to 29.93°.

Fig. 7 shows the tetragonal ZrO_2(111) diffraction peaks of the 9.5 nm-thick ZrO_2 films topped with various capping layers followed by PDA. It can be seen that the peak did not change when a 1.2 nm-thick TiO_2 layer was deposited on top, which implies that there was no interaction between the ZrO_2 and TiO_2 layers (lower two GIXRD data). The 1.2 nm-thick TiO_2 layer remains in the amorphous state after PDA. Even if the TiO_2 layer is crystallized, it has a different crystal structure (anatase or rutile) from the fluorite ZrO_2, so the TiO_2 and ZrO_2 cannot form the through-grains. One of the key findings from Fig. 4 and 6 was that the inserted dopant layer diffused when the upper and lower layers interacted with each other during the *in situ* crystallization or PDA. Therefore, it is likely that the Al–O and Y–O layers would not diffuse between the ZrO_2 and TiO_2 layers. Indeed, the ZrO_2(111) peak remained unchanged when the 2-cycle Al–O or Y–O layer was inserted (upper two GIXRD data). This result reconfirms that the dopant layer does not necessarily diffuse without the through-grain formation.

The results above indicate that the dopant diffusion occurs only when the dopant layer is within the bulk ZrO_2, which will hinder ZrO_2 through-grain formation if not diffused. However, it is questionable if the same phenomenon occurs when the dopant layer is interposed between the amorphous ZrO_2 layers

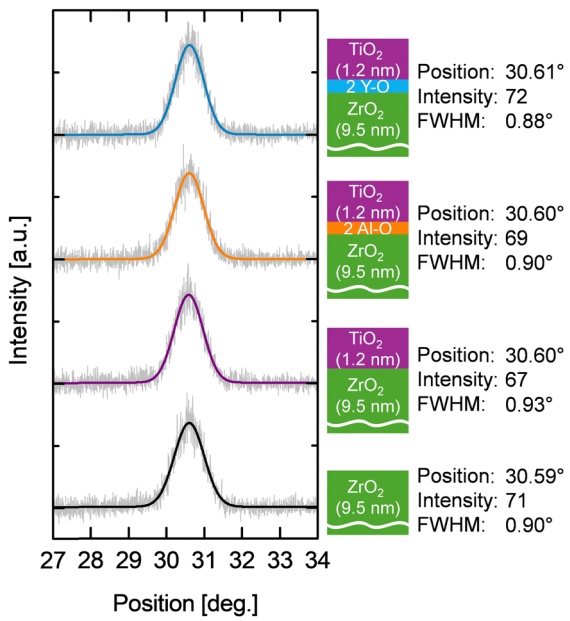

Fig. 7 GIXRD spectra showing the tetragonal ZrO_2(111) diffraction peaks of the 9.5 nm-thick ZrO_2 films topped with various capping layers. All film stacks were PDA treated, and the diffraction peaks were measured at an incident angle of 0.5° and Gaussian fitted. The peaks remain identical regardless of the capping layer materials, indicating no significant interaction between the ZrO_2 and each capping layer.

because the amorphous materials generally have a more open structure than the crystalline counterpart. Therefore, similar experiments were performed for the ZAZ samples, maintaining the amorphous structure even after PDA, which could be acquired by decreasing the total film thickness below the critical value. However, GIXRD cannot be used in this case. Therefore, X-ray photoelectron spectroscopy (XPS) is adopted to identify the chemical state of Al ions. The binding energy of the Al 2p spectrum shifts into the higher binding energy direction when it is diffused into the ZrO_2, so it can give accurate information on the Al diffusion.

Fig. 8 shows the XPS spectra of the four different film stacks: a PDA-treated 5.0 nm-thick crystalline bilayer film (named "[Z36A2]"), a sample with an additional 2-cycle Zr–O layer on top of [Z36A2] (named "[Z36A2]+Z2"), an amorphous as-deposited ZAZ film below the critical thickness ("Z7A2Z7", 2.2 nm), and finally, a PDA-treated Z7A2Z7 film (named "[Z7A2Z7]") which remained amorphous. The numbers in sample names represent the Zr–O and Al–O ALD cycles, and the square brackets indicate PDA treatment.

First, diffusion did not occur in [Z36A2], but it did occur in [Z36A2]+Z2 by the *in situ* crystallization of the top 2-cycle Zr–O layer, confirmed by GIXRD (data not shown). When comparing the XPS peaks, it was found that there were no differences in the Zr 3d and O 1s peaks between these two samples. The chemical bonding states of the surrounding Zr and O will change when Al ions are diffused. However, the portion of the entire ZrO_2 film collected by XPS is much larger than the amount of Zr and O affected, so no significant change is observed in the overall Zr 3d and O 1s peaks. However, the Al 2p binding energy in [Z36A2]+Z2 increased by ~0.19 eV compared to [Z36A2], indicating that Al diffusion into the ZrO_2 layer has occurred. This finding indicates that the Al 2p binding energy can be a feasible indicator for the Al diffusion. Fig. 8(a) (upper two data) shows that the amorphous Z7A2Z7 and [Z7A2Z7] samples exhibited the same Al 2p binding energy as [Z36A2], indicating no Al diffusion has occurred in both samples. The crystallinity might influence the XPS binding energy. However, it was reported that the Zr 3d and O 1s binding energies and the XPS spectra of an 8 nm-thick amorphous ZrO_2 film were identical to that of an annealed crystalline ZrO_2,[20] which can be further confirmed by the almost identical Zr 3d and O 1s binding energies observed in both the Z7A2Z7 and [Z7A2Z7] films to those of the [Z36A2] and [Z36A2]+A2 films. Therefore, it can be inferred that the Al 2p peak position accurately measures the Al diffusion into the ZrO_2 film. The diffused Al is expected to substitute neighboring Zr rather than being an interstitial, which was addressed through DFT calculations in the previous study.[12]

Experimental

ZrO_2-based films with various stack thicknesses were deposited *via* traveling-wave-type thermal ALD (Evertek) at a process temperature of 250 °C. The vacuum pressure was maintained

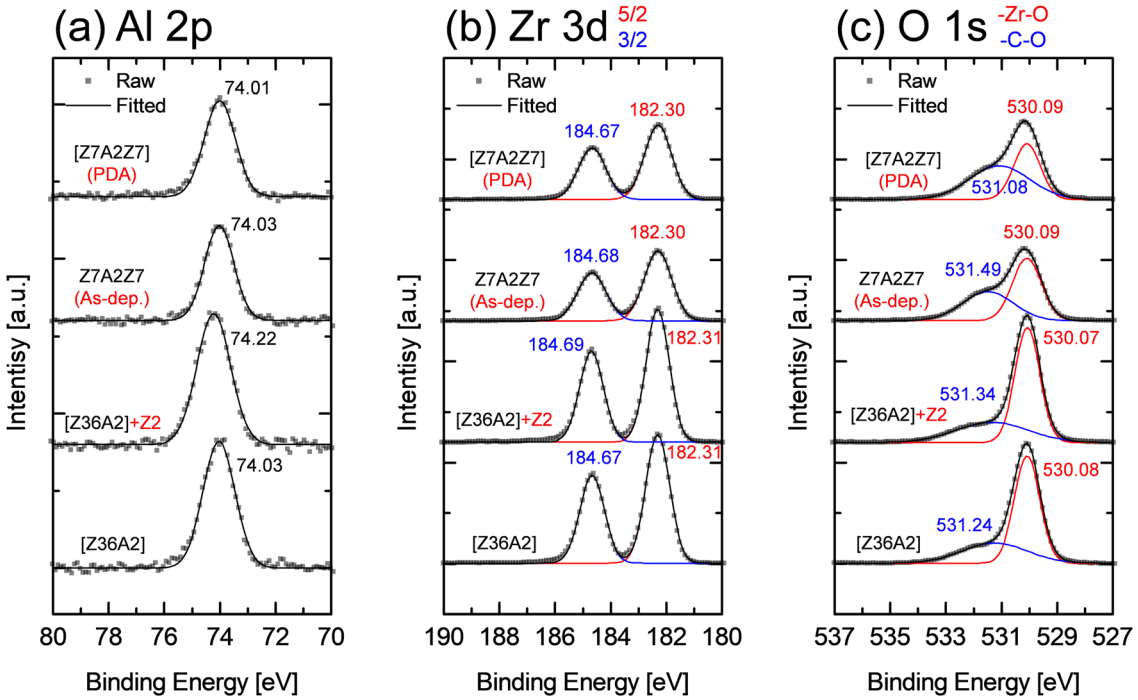

Fig. 8 XPS spectra of the four film stacks: a PDA-treated 5.0 nm-thick crystalline bilayer film (named "[Z36A2]"), a sample with an additional 2-cycle Zr–O layer on top of [Z36A2] (named "[Z36A2]+Z2"), an amorphous as-deposited ZAZ film ("Z7A2Z7", 2.2 nm), and finally, a PDA-treated Z7A2Z7 film (named "[Z7A2Z7]") which remained amorphous. The numbers in sample names represent the Zr–O and Al–O ALD cycles, and the square brackets indicate PDA treatment. (a) Al 2p, (b) Zr 3d and (c) O 1s spectra. The baseline was subtracted for all measured and fitted datasets. Al 2p's binding energy was higher only for the [Z36A2]+Z2 film, suggesting the substitution of Zr with Al (Al-diffusion effect).

under 30 mTorr before deposition. Heavily doped p-type Si wafers were used as the substrate. $Zr[N(CH_3)C_2H_5]_4$ (TEMAZr, 60 °C), $Al(CH_3)_3$ (TMA, 5 °C), $Y(EtCp)_2$(iPr-amd) (ARYA, 100 °C; manufactured by Air Liquide) and $Ti[OCH(CH_3)_2]_4$ (TTIP, 68 °C) were used as the Zr, Al, Y and Ti precursors. EtCp and iPr-amd indicate ethylcyclopentadienyl ($CH_2CH_3C_5H_5$) and isopropylamidinate ($CH(CH_3)_2CN_2CH_3$), respectively. Ozone (260 g m^{-3}) and Argon were used as oxygen source and carrier gas, respectively. Zr and Y precursors were delivered with the carrier gas at the flow rate of 100.0 SCCM. The deposition process followed the typical precursor pulse-purge-reactant pulse-purge sequence. The duration (in seconds) for each process step is as follows: Zr–O: 5–7–3–5 (s), Al–O: 0.5–25–3–5 (s), Y–O: 5–17–3–5 (s) and Ti–O: 3–5–3–5 (s).

The Al–O and Y–O layer thicknesses were estimated from the measured growth rates of each layer on ZrO_2, which were approximately 0.10 nm $cycle^{-1}$ and 0.15 nm $cycle^{-1}$, respectively. The total thickness and each layer's physical thickness were measured using the spectroscopic ellipsometry (SE; M-2000, J. A. Woollam) and the areal-density (μg cm^{-2}) data obtained from the X-ray fluorescence spectroscopy (XRF; Quant'X, Thermo Scientific).

All samples underwent PDA *via* the rapid thermal annealing process at 600 °C (with N_2 gas) to crystallize the dielectric layer, except for the samples in Fig. 4 and 8, where the annealing methods are specifically described. All PDA treatments included dopant layers to induce their potential dopant diffusion.

GIXRD was conducted *via* an X-ray diffractometer (XRD; X'pert Pro, PANalytical) for crystal structure and diffusion behavior analyses. The omega alignment was performed until the margin was reduced to less than 0.010°. The scan step size and time-per-step were set to 0.005° and 0.50 s, respectively. All diffraction peaks were Gaussian fitted (single peak) after subtracting background intensities. The tetragonal ZrO_2 phase and continuous grain formation were reconfirmed *via* high-resolution transmission electron microscopy (HRTEM; JEM-ARM200F, JEOL). Details and reliability of the GIXRD analysis are explained in ESI.†

X-ray photoelectron spectroscopy (XPS; ESCA Axis Supra+, Kratos) was used to identify the chemical states of Zr, Al and O ions in amorphous ZrO_2 films. Binding energies were calibrated with the standard C 1s peak at 284.8 eV.

Conclusions

This study examined the diffusion behaviors of Al and Y dopants in different configurations of ZrO_2 thin films grown by ALD. Due to the smaller and larger ionic radii of Al and Y than Zr, local lattice contraction and expansion, respectively, occurred when they were diffused into ZrO_2, as evidenced by shifts in X-ray diffraction peaks. However, substitutional diffusion of both dopants occurred only when the dopant layer was embedded within the ZrO_2 layer (*i.e.*, ZAZ or ZYZ stack), essentially obstructing the ZrO_2 grain growth at the inserted location. The Al–O and Y–O layers deposited on top or at the

bottom of the ZrO_2 layer (*i.e.*, ZA or ZY bilayer stack) did not diffuse into the adjacent ZrO_2 lattice.

This peculiar behavior was attributed to the close relationship between interdiffusion and ZrO_2 grain growth during crystallization. From the interface (or grain boundary) energy perspective, it was energetically favorable for ZrO_2 films to form through-grain structures, where there was a crystallographic continuity between the adjacent ZrO_2 layers. However, Al readily diffused when a thin (<0.3 nm) Al–O intervening dopant layer existed within the ZrO_2.[12] This diffusion removed the obstacle to developing the through-grain structure. In other words, the formation of these through-grains is a factor that promotes the diffusion of Al. This effect occurred even with just a single monolayer of Zr–O covering the Al–O layer on the opposite side of the crystallized ZrO_2 layer. However, when the embedded Al–O layer was thick (>0.3 nm), it completely disrupted the interaction between the upper and lower ZrO_2 layers, prohibiting the through-grain formation. In this case, the driving force for the Al diffusion disappeared, allowing the thick Al–O layer to remain intact. As a result, the ZrO_2 layer eventually separated into two layers.[12]

In contrast, the interposed Y–O layer inside the ZrO_2 layer was readily diffused regardless of its thickness due to its high solid solubility and diffusivity, allowing through-grain formation. However, the Y diffusion did not occur when the Y–O layer was outside the ZrO_2 film despite its high solid solubility and diffusivity, signifying that the most crucial parameter for the Al and Y diffusion is the through-grain formation. A similar effect was observed in the amorphous material. Despite the more open structure of the amorphous ZrO_2 film, achieved by lowering its thickness below the critical thickness for crystallization under the given PDA conditions, no Al diffusion was identified through XPS even when the A–O layer was embedded in the amorphous ZrO_2 film.

These findings indicate that the primary driving force for the Al and Y dopant diffusion in such nano-scale ZrO_2 thin films is eliminating the grain boundary energy by forming the through-grains, not the concentration gradient.

Author contributions

H. Seo designed and performed the experiments and wrote the manuscript. J. Shin, H. S. Park, T. K. Kim, H. Paik and H. Song helped the data interpretations and reviewed the manuscript. C. S. Hwang supervised the whole research and manuscript preparation.

Data availability

All data generated or analyzed during this study are included in the main article and ESI.† The data that support the findings of this study are available from the corresponding author upon reasonable request.

Conflicts of interest

There are no conflicts to declare.

Acknowledgements

This work was supported by (1) the Korea Evaluation Institute of Industrial Technology through the Technology Innovation Program (No. 20017216) and (2) SK Hynix Inc. under its Center of Material Research for Semiconductors (C-MRS) program.

Notes and references

1 R. B. Bird, W. E. Stewart and E. N. Lightfoot, *Transport Phenomena*, John Wiley & Sons, 2006.
2 A. A. Malygin, V. E. Drozd, A. A. Malkov and V. M. Smirnov, *Chem. Vap. Deposition*, 2015, **21**, 216.
3 R. L. Puurunen, *Chem. Vap. Deposition*, 2014, **20**, 332.
4 M. Ritala and M. Leskela, *Atomic Layer Deposition, Handbook of Thin Film Materials: Deposition and Processing of Thin Films*, Academic Press, 2002, 103.
5 M. Gutsche, H. Seidl, T. Hecht, S. Kudelka and U. Schroeder, Atomic Layer Deposition for advanced DRAM applications, *Future Fab. Int.*, 2003, **15**, 1.
6 R. C. Garvie, *J. Phys. Chem.*, 1965, **69**, 4.
7 R. C. Garvie, *J. Phys. Chem.*, 1978, **82**, 2.
8 H. J. Cho, Y. D. Kim, D. S. Park, E. Lee, C. H. Park, J. S. Jang, K. B. Lee, H. W. Kim, Y. J. Ki, I. K. Han and Y. W. Song, *Solid-State Electron.*, 2007, **51**(11), 1529.
9 D. Martin, M. Grube, W. Weinreich, J. Muller, W. M. Weber, U. Schroder, H. Riechert and T. Mikolajick, *J. Appl. Phys.*, 2013, **113**, 194103.
10 M. Pesic, S. Knebel, M. Geyer, S. Schmelzer, U. Bottger, N. Kolomiiets, V. V. Afanas'ev, K. Cho, C. Jung, J. Chang, H. Lim, T. Mikolajick and U. Schroeder, *J. Appl. Phys.*, 2016, **119**(6), 064101.
11 M. Pesic, S. Knebel, K. Cho, C. Jung, J. Chang, H. Lim, N. Kolomiiets, V. V. Afanasev, T. Mikolajick and U. Schroeder, *Solid-State Electron.*, 2016, **115**, 133.
12 H. Seo, I. W. Yeu, D. S. Kwon, D. G. Kim, J. Lim, T. K. Kim, H. Paik, J.-H. Choi and C. S. Hwang, *Adv. Electron. Mater.*, 2022, **8**, 2200099.
13 S. H. Cha, C. H. An, S. T. Cho, D. Kim, D. S. Kwon, J. I. Lim, W. Jeon and C. S. Hwang, *Phys. Status Solidi RRL*, 2019, **13**, 1900282.
14 H. Seo, H. S. Park, S. T. Cho, J. Shin, J. Lim, T. K. Kim, H. Paik, H. Song and C. S. Hwang, *J. Appl. Phys.*, 2024, **136**, 1.
15 K. Oura, M. Katayama, A. V. Zotov, V. G. Lifshits and A. A. Saranin, *Surface Science: An Introduction*, Springer, 2003.
16 W. D. Nix and B. M. Clemens, *J. Mater. Res.*, 1999, **14**, 3467.
17 R. C. Cammarata, T. M. Trimble and D. J. Srolovitz, *J. Mater. Res.*, 2000, **15**, 2468.
18 R. A. Miller, J. L. Smialek and R. G. Garlick, *J. Am. Ceram. Soc.*, 1981, **3**, 241.
19 D. A. Jerebtsov, G. G. Mikhailov and S. V. Sverdina, *Ceram. Int.*, 2000, **26**, 821.
20 D.-Y. Cho, H.-S. Jung, J. H. Kim and C. S. Hwang, *Appl. Phys. Lett.*, 2010, **97**, 141905.

